Mem. Fac. Eng., Kyoto Univ., Vol. 57, No. 2 (1995)

Molecular Dynamics Study of Small-Size Argon Clusters: Effects of Three-Body Interaction on Structure, Dynamics and Phase Transition

By

Koichiro NAKANISHI* and Kazuhiro NOMURA#

(Received October 21, 1994)

Abstract

Molecular dynamics simulations have been carried out for small-size argon clusters. The number of molecules in the clusters is between 12 and 20. In order to study rather dense structures of clusters at lower temperatures, effects of the Axilrod-Teller type three-body interaction on the structure and dynamics of the clusters have been examined in detail. In addition to conventional MD calculations, we have performed quenching of clusters to obtain some inherent structures of the clusters. We have further carried out normal mode analysis and discussed the origin of the appearance of "magic number" clusters. It is found that the three-body effect does exist in various properties but they are not large as to alter our qualitative picture and the cluster size dependence.

1. Introduction

Micro-clusters composed of a small number of particles exhibit various unique properties which are different from those of bulk phases because a large fraction of the particles is in the surface region. Studies of such clusters are motivated by the interest in their structures, the initial stages of crystal growth, the possibility to the presence of phase transitions and many other. Many studies on micro-clusters have focused attention to the rare gas for which both experimental and computational results are abundantly available. According to the evidence from mass spectral measurements[1,2], the stability of clusters becomes larger for some specific sizes. They are called Magic Number (MN) clusters. While such evidence is mostly for charged clusters, the stability of neutral clusters should have a close connection with the presence of MN. Furthermore, electron diffraction studies show that the structure of clusters composed of several hundreds molecules is different from that of crystal but similar to that of amorphous metals[3].

Computational studies on the structure and transition of rare gas clusters have been carried out during the past two decades by using both molecular dynamics (MD)[4,5] and

Department of Polymer Chemistry and Division of Molecular Engineering
* To whom correspondence should be addressed.
# Present address: NEC Co., Shiba 5-7-1, Minato-ku, Tokyo 108-01, Japan.

Monte Calro (MC)[6,7] methods with conventional two-body Lennard-Jones (LJ) potential for molecular interactions. As for the structure, Hoare et al.[8] have shown that the stable forms of rare gas clusters with several ten molecules look like the icosahedron (ICS) structure rather than the face-centered cubic (FCC) form as in the bulk phases. This stimulates the calculations for determining the cluster size, at which the FCC structure becomes more stable than the ICS structure[9,10], because this is very important in crystal growth studies. More recently, Berry et al.[11] and Wales[12], among others, have carried out more elaborate calculations in small size rare gas clusters and confirmed from MD calculations that a transition-like phenomenon occurs when the temperature of MN clusters increases. This kind of "transition" is somewhat different from the phase transition in bulk systems and, in spite of some detailed analyses, its nature is still unknown. The presence of such phase transition-like behavior in small-size clusters is extremely interesting from the thermodynamic point of view. For example, no such 'transitions' are observed for non-MN clusters. These indicate that the properties of clusters depend on whether they are MN or not. It is thus quite challenging to investigate the reason why a group of molecules composed of some specific number hehaves like an MN cluster.

With the situation discussed above in mind, the present cluster study includes the following MD and related computations:

1) Both two-body and three-body potentials have been used in order to estimate the degree of possible many-body effects in various properties of micro-cluster systems[12,13].
2) Conventional MD computations for the structure and phase transition in small size (12–19 molecules) clusters.
3) The quenching of the configurations of molecules in the cluster to obtain 'inherent' structure and to perform normal mode analysis.
4) The comparison and mutual transformation between ICS and FCC structures.

Although the scope of the present study is more and less overlapped with those of recent works by Berry[11] and Wales[12], among others, it should be helpful to establish a detailed picture for small size LJ clusters with 7 to 20 molecules.

In section **II** the three-body interaction used in the present study is described. After explaining the method of computation adopted here in section **III**, we present our main results in section **IV** and finally concluding remarks are given in section **V**. Three brief Appendixes are also included.

2. Three-body interaction

The potential energy of classical systems composed of N particles can generally be written in a series expansion form.

$$U=\frac{1}{2!}\sum_{\substack{i=1\\ i\neq j}}^{N}\sum_{j=1}^{N}u_{ij}+\frac{1}{3!}\sum_{i=1}^{N}\sum_{\substack{j=1\\ i\neq j\neq k}}^{N}\sum_{k=1}^{N}u_{ijk}+\cdots$$
$$+\frac{1}{n!}\sum_{i=1}^{N}\sum_{\substack{j=1\\ i\neq j\neq\cdots\neq n}}^{N}\cdots\sum_{n=1}^{N}u_{ij\cdots n}+\cdots \tag{1}$$

The leading term in the RHS of Eq. (1) is the two-body interaction. A typical example of the potential truncated after second and further terms is the Lennard-Jones (LJ) 12-6 potential,

$$U_{LJ}(r_{ij})=4\varepsilon\left\{\left(\frac{\sigma}{r_{ij}}\right)^{12}-\left(\frac{\sigma}{r_{ij}}\right)^{6}\right\} \tag{2}$$

which is proved to be suitable for rare gases. We will use this potential as a reference to measure possible three-body effects which appear in the dense cluster structures at lower temperatures. The parameter values used are $\varepsilon=0.996$ kJ mol^{-1} and $\sigma=3.405$ A.

The Axilrod-Teller (AT)[14] potential,

$$U_{AT}(r_{ijk})=\nu\frac{(1+3\cos\theta_i\cos\theta_j\cos\theta_k)}{(r_{ij}r_{ik}r_{jk})^3} \tag{3}$$

has been used for three-body interaction in rare gas systems. In this equation, ν is a constant depending on polarizability and $\nu^*=\nu/(\varepsilon\sigma^9)=0.0719$, r_{ij} the intermolecular distance between i and j and θ_i the angle between j and k. The AT potential U_{AT} can be either positive or negative, depending on the triangle ijk formed. However, it is mostly positive, in other words, it acts generally as a repulsive interaction. It is of short range nature, as compared with the two-body interaction. In the present calculation, we will use LJ+AT (LA) potential to evaluate the effect of three-body interactions. The most stable structures for three rare gas molecules are of the normal triangle both with LJ and LA potentials. The length and minimum energy are as below.

LJ: r=0.3820 nm and E=-2.998 KJ mol^{-1}
LA: r=0.3827 nm and E=-2.958 KJ mol^{-1}

These differences might be rather small. We will therefore use another artificial potential LJ+4AT, where an over-emphasized three-body term is adopted.

The first-order differential form of the AT potential necessary for the calculation of inter-particle forces in MD simulation is given in the **Appendix I.**

3. Method of computation

Conventional MD simulation programs within an NEV ensemble have been used throughout the calculation with the following modifications for clusters:

1. Periodic boundary condition is removed to deal with free clusters.
2. No potential truncation is applied for small size clusters.
3. For each size of cluster, the most stable structure obtained in advance is used as the initial configuration.
4. Initial velocities are given so as to prevent the translation and rotation of the whole cluster.

The equations of motion for the molecule forming cluster were solved numerically by using the difference equation originally proposed by Verlet[15]. The time step Δt in the MD simulation was 0.01 ps and the total number of time steps were 60,000 to 100,000. When the three-body term was involved, a large CPU time was required. The temperature obtained by this calculation is simply the kinetic energy defined by

$$T=\frac{2}{(3N-6)}\frac{<KE>}{k} \tag{4}$$

Since the translational and rotational motions of the whole cluster are excluded, the corresponding degrees of freedom are removed from the equation.

4. Results and discussion

A. Stable structure of clusters

The most stable structure and its potential energy value have been determined for Lennard-Jones argon clusters composed of 6 to 20 molecules in order to confirm previous calculations[8a]. Both LJ and LA models have been used. The process of the determination of the most stable structure is as follows. We first perform MD calculations at relatively high temperatures for several thousand time steps and then, based on some MD data, "quenching" procedures are appled to obtain the corresponding "inherent structures" at the potential minimum. Finally, we seek the structure having the lowest potential energy. As a result, each cluster with the most stable structure has been obtained. Although the number of potential minimum structures becomes increasingly larger as the cluster size increases, we determined the most stable structure, because these structures can be predicted to some extent as they are close to being in an eicosahedron form and the inherent structures corresponding to them will appear rather frequently. As is already known, smaller clusters prefer the ICS structure rather than the FCC structure[8a]. These are some of the reasons why our prediction is often successful.

Table 1. The minimum potential energies for the Ar clusters interacting with LJ or LA potential.

N	6	7	8	9	10
LJ	−12.661	−16.439	−19.743	−24.017	−28.309
LA	−12.267	−15.879	−19.060	−23.134	−27.218

N	11	12	13	14	15
LJ	−32.635	−37.816	−44.150	−47.654	−52.114
LA	−31.329	−36.203	−42.112	−45.490	−49.744

N	16	17	18	19	20
LJ	−56.589	−61.073	−66.265	−72.369	−76.868
LA	−54.009	−58.286	−63.154	−68.847	−73.136

(kJ/mol)

The minimum values E_{min} of the potential energy are shown in Table 1 and plotted against the number fo molecules in clusters N in Fig. 1. The energy difference between two consecutive clusters, $\triangle U = U(N) - U(N-1)$, are also plotted in Fig. 2. The absolute value of $\triangle U$ corresponds to the energy required to remove one molecule from the cluster composed of N molecules. As is seen in Fig. 2, $|\triangle U(N)|$ shows deep minima at N=13 and N=19, indicating the large relative stability of these clusters. This is to be compared with higher peaks in the mass spectra for charged clusters. Although the effect of the

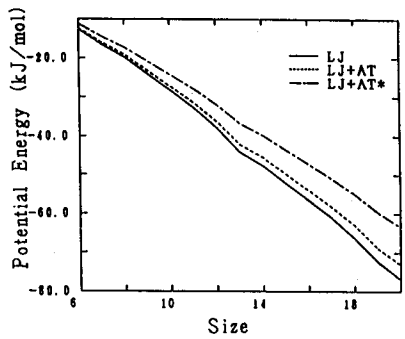

Fig. 1. Potential energies *vs* number of atoms in the clusters. AT*=4AT potential.

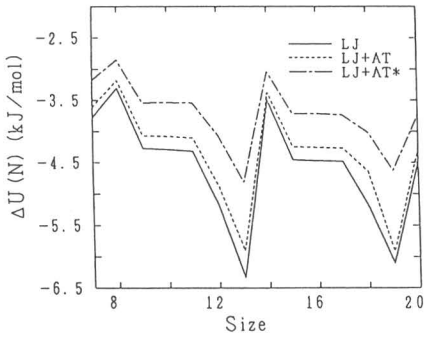

Fig. 2. The difference in the potential energies between Ar_N and Ar_{N-1} clusters. AT*=4AT.

three-body term becomes more significant for the region in which $|\triangle U(N)|$ is larger, the general aspect of size dependence remains unchanged. In other words, although the three-body term has a fairly large influence on the stable structure of clusters, it is not large enough to change the order of the relative stability of the clusters. As seen in Table 1, relative stability does not change even when we use stronger 4 AT potential.

The minimum energy structures of small LJ clusters have already been known. The inclusion of AT term (LA) do not change the minimum energy structures for the clusters studied. The most stable structures of representative LJ Ar clusters are given for the selected N values in Fig. 3. No appreciable differences in fundamental structure are found between LJ and LA clusters, though the latter shows a relatively expanded form.

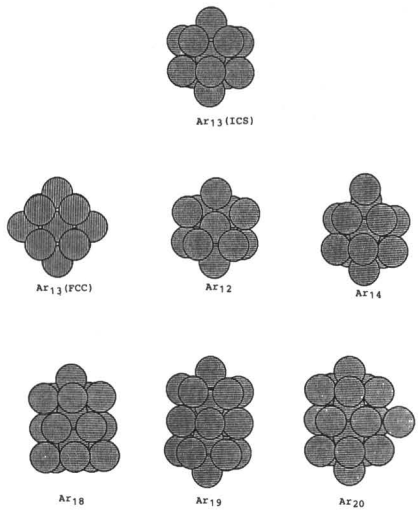

Fig. 3. The most stable structures of Ar_N clusters. ICS structure is more stable than FCC structure for Ar_{13} clusters.

Further discussion on the Ar_{13} cluster is given in **Appendix II** because this includes some already known results.

B. Phase transition in cluster

The phase transition in cluster has been studied extensively by Berry et al.[11] However, the nature of transition phenomena is still not fully understood.

The melting of clusters, Ar_{12}, Ar_{13}, Ar_{14}, and Ar_{19}, is shown in Figs. 4 and 5, where the total energy E_t per particle and the fluctuation of bond distance δ are plotted against temperature, respectively. The parameter δ, which is defined as

$$\delta=\frac{2}{N(N-1)}\sum_{i<j}\frac{(<r_{ij}^2>-<r_{ij}>^2)^{1/2}}{<r_{ij}>} \tag{5}$$

is sensitive to the structural change in the cluster. One can see in Fig. 4 that E_t changes smoothly with temperature for Ar_{12} and Ar_{14} clusters, while first-order transition-like behavior is observed for Ar_{13} and Ar_{19} clusters, in other words, there exists a plateau in E_t vs. T curve. However, the slope of E_t vs T plot at lower temperature is different from that at higher temperature. The difference in the slope means the change in the heat capacity. Clearly, the thermodynamic states of the cluster are different. Moreover, although δ changes monotonically at lower temperatures, it becomes suddenly significant at certain temperatures. This is similar to the Lindemann rule in the crystalline state. The observed large jump in δ is especially remarkable for Ar_{13} and Ar_{19}. Since the change in δ indicates a large change in inter-particle distance, the occurrence of a large structural change is expected. Phase transition-like behavior does exist certainly in the clusters of this size and no continous change occurs in the transition from solid-like to liquid-like structure. Hereafter we will discuss such structural changes which might be called "cluster transition".

The effect of the three-body term is a decrease in the transition temperature for all sizes of cluster. The transition occurs at abbout 34 K for Ar_{13} and Ar_{19} with the LJ potential, while the transition temperature becomes 31 K for clusters with the LA potential. The temperature decrease seems to be relatively large for Ar_{19}. This transition temperature coincides with the temperature where the exchange of the central molecule begins to occur. Contrary to the very small effects of the three-body term on the structure and energy of the cluster, this temperature decrease is rather large. This can be more clearly seen by strengthening the three-body term. However, the nature of the dynamics of transition is almost the same both with LJ and LA intractions. We therefore confine ourselves to the transition in the cluster with LJ potential, examine the difference between MN and non-MN clusters in detail, and discuss the reason that the three-body term could lower the transition temperature. Detailed analyses are made for the transitions in Ar_{13} MN cluster, and Non-MN Ar_{12} and Ar_{14} clusters with the LJ poten-

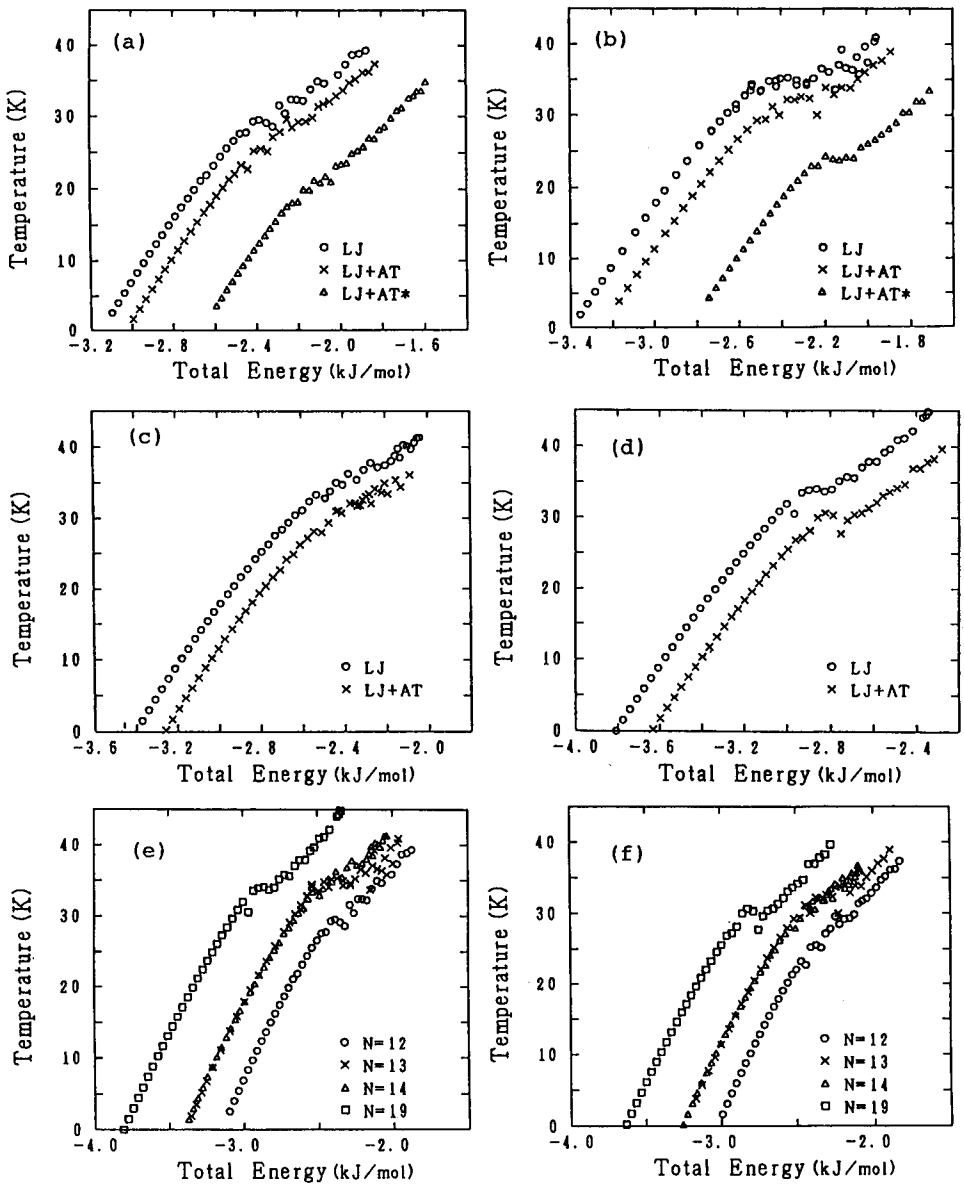

Fig. 4. Caloric curves for several cluster sizes.
(a) Ar_{12} (b) Ar_{13} (c) Ar_{14} (d) Ar_{19} (e)LJ clusters (f) LA clusters

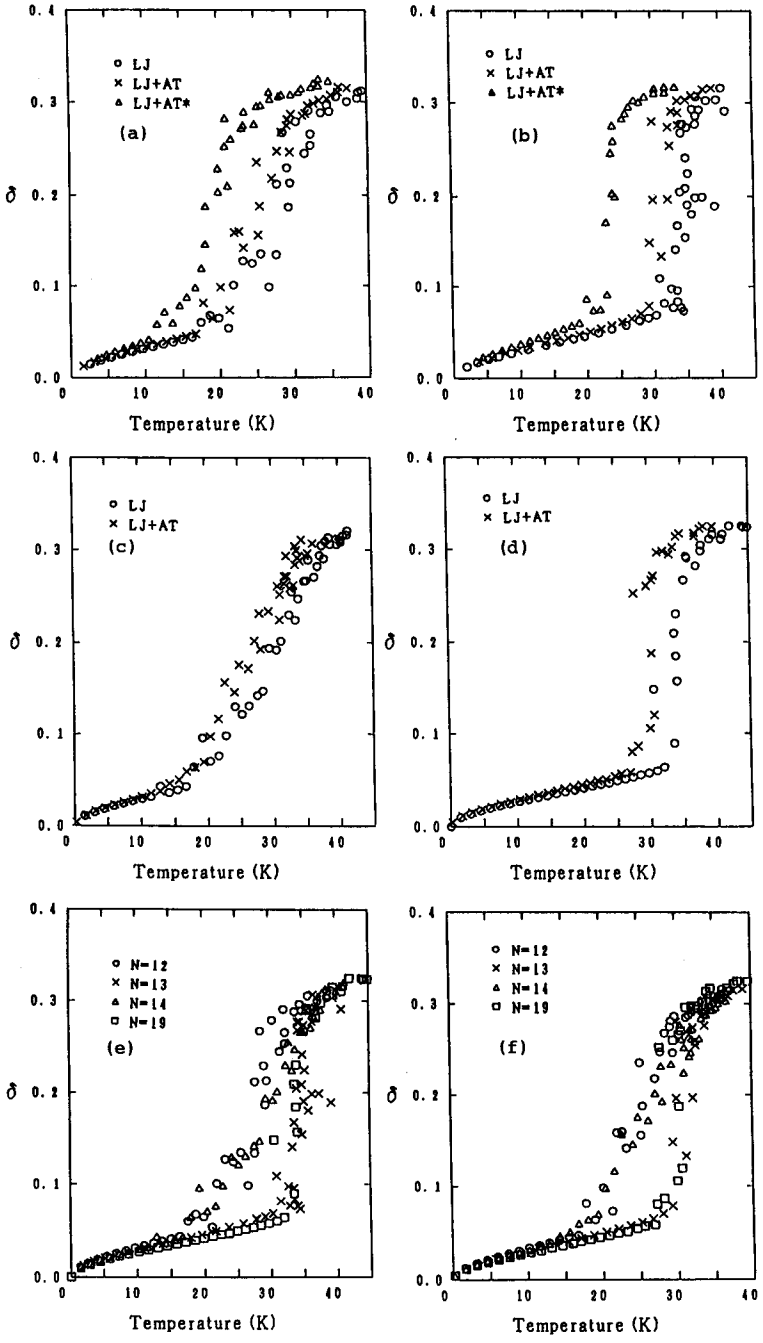

Fig. 5. Relative root-mean-square bond length fluctuations for several cluster sizes. (a) Ar_{12} (b) Ar_{13} (c) Ar_{14} (d) Ar_{19} (e)LJ clusters (f) LA clusters

tial. Since some of the materials used here are already available in literature, we give the details in **Appendix III.**

C. Quenching

We carried out the procedure of quenching to obtain inherent structures and their potential energies in each local minimum of the potential energy surface.

As is originally proposed by Stillinger and Weber[16], the quenching can be done by solving, instead of the Newton equations of motion, the following equation,

$$\dot{\mathbf{r}} = -\nabla U(\mathbf{r}) \tag{6}$$

The energy of the system can be decreased to a local minimum by moving all the particles from an equilibrium configuration at a given temperature to the direction of the force exerted. This procedure is repeated many times from different configurations and the energy distributions for the inherent structures thus obtained are shown for the four Ar clusters in Fig. 6. The lowest energy value is arbitrarily taken as zero and the difference from it is given for each structure. The number of inherent structures is 101 for Ar_{12}, 118 for Ar_{13}, 112 for Ar_{14} and 280 for Ar_{19}, respectively. The actual number of inherent structures should be larger than that studied here. However, we believe that most important inherent structures with lower energy values have been included in the present calculation. Therefore, the distribution obtained should be almost the same as the real one except for the higher energy side.

Information obtained from Fig. 6 may be summarized as below.

1. The difference between the minimal potential energy and the next minimum energy depends on the size of the cluster (see Table 2).
2. When the number of such next minimum energy levels is two or more, there is a longer energy gap to the next energy level.

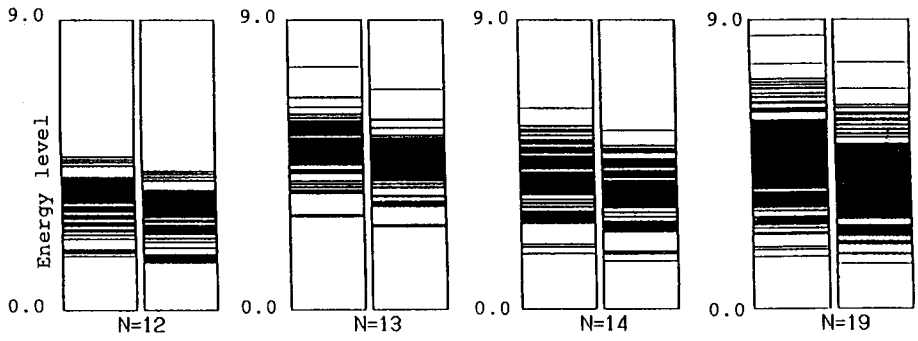

Fig. 6. The energy levels of the potential minima. Left side is for LJ cluster and right side is for LA cluster. The energy unit is in kJ/mol.

Table 2. The energies of the lowest potential minima and the next potential minima and their differences in Ar clusters interacting with LJ or LA potential.

N	12	13	14	19
LJ	−37.816 −36.162	−44.150 −41.306	−47.655 −45.978	−72.369 −70.799
	△U=1.654	△U=2.844	△U=1.677	△U=1.570
LA	−36.203 −34.734	−42.112 −39.566	−45.490 −44.050	−68.847 −67.474
	△U=1.469	△U=2.546	△U=1.440	△U=1.373

(kJ/mol)

Thus, the effect of the three-body term is appreciable for high energy regions. When quenching is carried out, there is almost no reversal of the energy level of "inherent structure" between LJ and LA models. Such reversal may occur in high energy regions where energy level differences are small.

D. Further consideration of the transition

It is a feature of the potential surface of MN clusters that the energy corresponding to the minimum energy structure is somewhat smaller than those for other structures. In order to examine the relation of this feature with the transition, quenching has been carried out by using the previous MD data (each separated by 500 steps) which are used to obtain APE distribution (see Appendix III). From the energy of the quenched states, the APE and trajectories of particles, we discuss the nature of the transition in more detail.

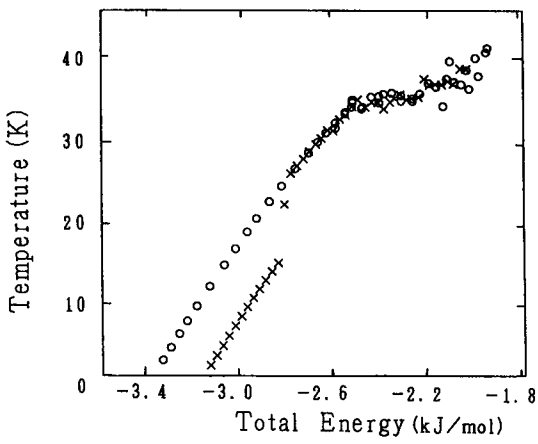

Fig. 7. Caloric curves fo Ar_{13} cluster with LJ potential. Circles are started from icosahedron structure and crosses are started from the second lowest structure.

The change of energies in the inherent structure is shown later in Fig. A6.

It is seen that the inherent structure for Ar_{13} changes with APE. That for lower energy is of ICS structure. Furthermore, those structures having higher APE at 33 K lead to the three inherent structures with fairly high probability. At this temperature it is not easy to transfer to a higher energy minimum. These three inherent structures correspond to the three energy levels located near the second lowest minimum in Fig. 6. These structures can be constructed by taking one molecule from thirteen surface molecules in Ar_{13} and putting it on the surface. There are three different ways to do so and their structures are fairly stable. Using one of these structures as the initial configuration, we calculated the potential energy curve as in Fig. 7. This should be closely related to the transition, though the interpretation is difficult.

We have made an approximate calculation on the probability that the cluster structure takes one of these three inherent structures. This involves a large scale MD calculation and subsequent quenching. Similar calculations have also been done with Ar_{12}, Ar_{14} and Ar_{19}. The results are summarized in Table 3. Here we define three kinds of energy level from the energy distribution in Fig. 6. They are the lowest minimum (E_1), the next (second lowest) minima (E_2), and others (E_3), respectively. Cluster size dependence appears with the increase in temperature. The feature of the MN Ar_{13} cluster is that the level E_3 is rarely occupied. In the cases of non-MN Ar_{12} and Ar_{14}, the occupancy ratio of E_3 level is rather high. These facts suggest that there is a large difference between MN and non-MN clusters and that the MN cluster is highly stable. Both the lowest minimum and the second lowest minima occupy large volumes in the phase space.

As in seen in the above discussion, the structural transition is closely related to that between potential energy minima. A plausible picture might be such that, before the transition, there exists only an intermolecular vibrational motion around a potential energy minimum characterized by a specified temperature and potential energy, and that, after the transition, free transitions among various minima can be allowed with averaged temperature and energy. In the intermediate region, three kinds of energy levels are in equilibrium with each other[17] and the temperature of the cluster and other properties should be dependent on this equilibrium. The equilibrium for MN clusters is different (e.g, the presence of first order transition like plateau) from that for non-MN clusters. The reason that the introduction of the three-body term leads to the decrease in transition temperature may be explained by the fact that the transition is assumed simply as that from the most stable potential minimum to the next minima. Owing to the presence of a potential barrier between the two minima, some kinetic energy must be necessary. As was pointed out before, the energy difference between potential minima tends to be smaller under the influence of the three-body term. Probably the potential barrier will also become lower and the transition is possible with less kinetic energy, namely, at lower

Table 3. The fractions of each energy level for several kinds of energies. A, B, C... correspond to each different temperature as the transition proceeds

		E_t (kJ/mol)	E1 (%)	E2 (%)	E3 (%)
Ar_{12}	A	−2.57	100	0	0
	B	−2.44	97	1	2
	C	−2.41	84	12	4
	D	−2.35	70	18	12
	E	−2.29	65	25	10
	F	−2.23	51	22	27
	G	−2.14	45	25	30
	H	−2.07	31	27	42
	I	−2.00	37	26	37
Ar_{13}	A	−2.69	100	0	0
	B	−2.61	100	0	0
	C	−2.57	95	5	0
	D	−2.50	84	6	10
	E	−2.49	82	18	0
	F	−2.42	73	24	3
	G	−2.37	57	25	18
	H	−2.33	51	29	20
	I	−2.25	46	31	24
	J	−2.18	39	33	28
Ar_{14}	A	−2.69	100	0	0
	B	−2.56	88	11	1
	C	−2.49	90	8	2
	D	−2.46	78	14	8
	E	−2.43	77	3	20
	F	−2.38	72	7	21
	G	−2.30	64	13	23
	H	−2.24	49	13	38
	I	−2.17	45	12	43
	J	−2.13	51	14	35
Ar_{19}	A	−3.07	100	0	0
	B	−3.00	99	0	1
	C	−2.96	60	38	2
	D	−2.93	57	24	19
	E	−2.90	53	32	15
	F	−2.86	37	41	22
	G	−2.79	18	34	48
	H	−2.72	7	23	70
	I	−2.65	11	17	72
	J	−2.52	6	13	81

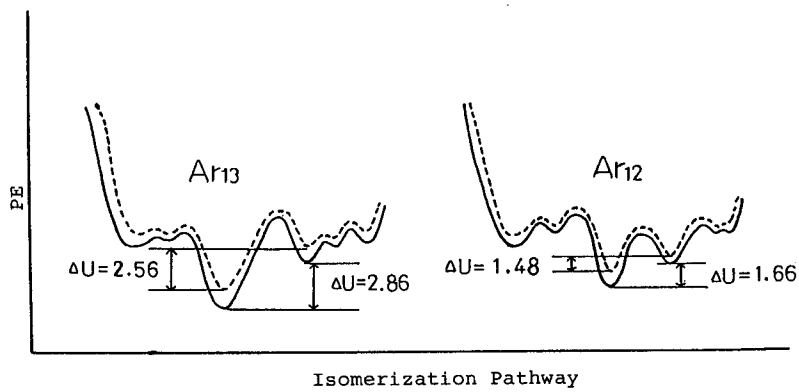

Fig. 8. The model potential surfaces for Ar_{12} and Ar_{13} clusters.
—— LJ model and ----- model

temperature. Fig. 8 illustrates this situation. However, further calculation is necessary to evaluate the height of the potential barrier, though such an attempt is already available[18].

E. Normal mode analysis

Normal mode analysis has been carried out for the four argon clusters using the inherent structures obtained by quenching. Only the LJ potential is used at present. The resultant wave number distribution is shown in Fig. 9. The size dependence of this distribution cannot be clearly seen from this figure. However, the distribution increases in the low wave number region for Ar_{19}. For all the clusters studied, the distribution is concentrated in the high wave number region for lower energy structures and no high wave number contribution for higher energy structures and the concentration of the highest wave number structure is from the most stable one. The wave number distribution for the most stable structure is such as that in Fig. 10. As is seen from Fig. 10, the low wave number region for Ar_{13} has a larger distribution as compared with other clusters. This is usually one feature of MN clusters.

F. Comparison between ICS and FCC structures

While the clusters composed of a few hundred molecules have the ICS structure, the crystal structure of Ar is of FCC form. It is thus of interest to know the cluster size at which the transition occurs between them from the standpoint of the crystal growth[17]. Experimental evidence is also available from electron diffraction study[9]. The results are, however, confusing. According to the recent reports, it is as large as $4 \times 10^3 \sim 10^4$ [10]. The calculation with the LA potential needs an extaordinarily large computing time and we have presently made no attempt to perform such calculation. In view of the results for Ar_{13}, however, the transition from ICS to FCC structure should occur earlier. In

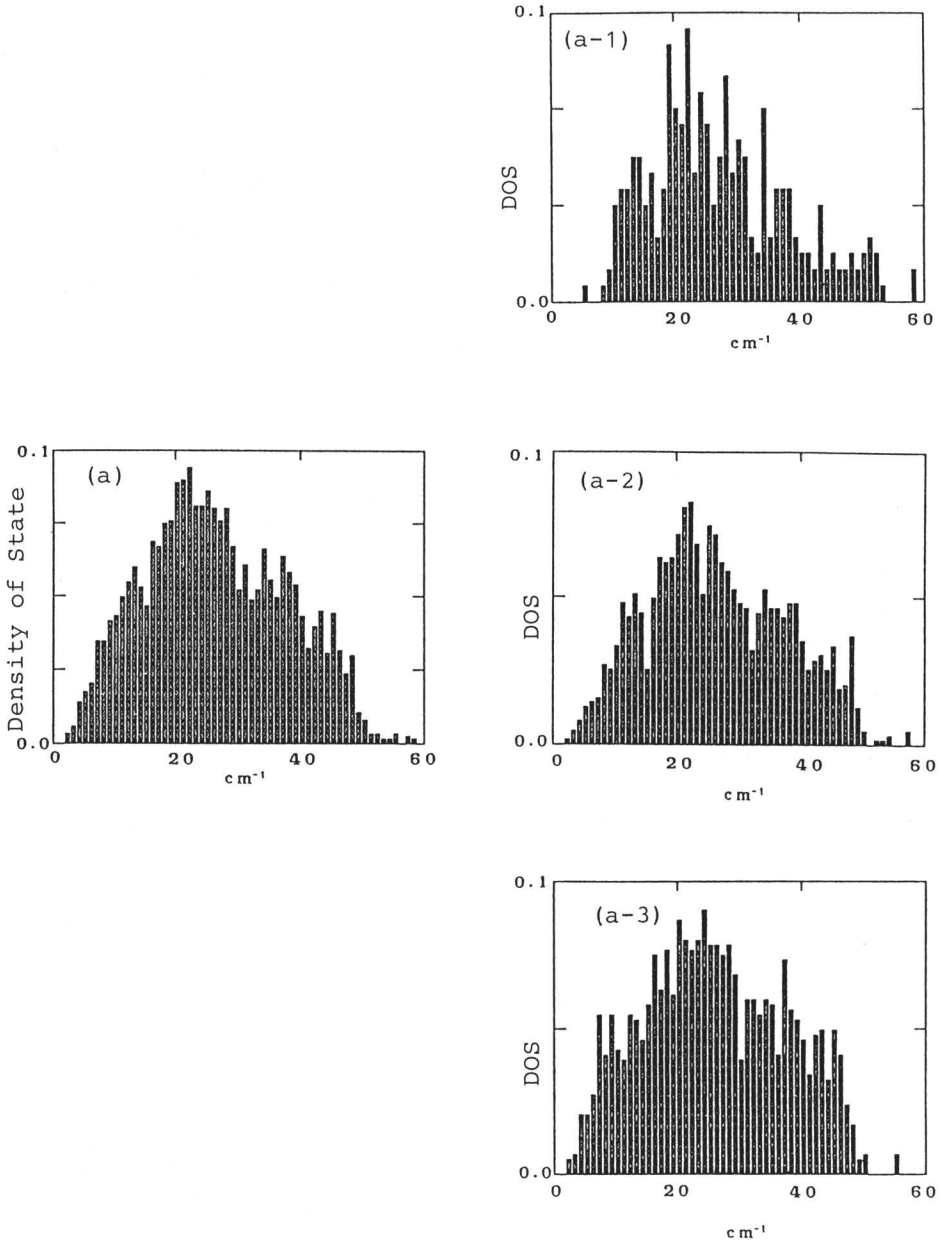

Fig. 9. Normal mode historgrams. (a) Ar_{12}, (b) Ar_{13}, (c) Ar_{14}, (d) Ar_{19}. (a-1)~(a-3) are calculated separately in each energy level, 1 (low), 2 (middle), and 3 (high) potential energy levels, respectively.

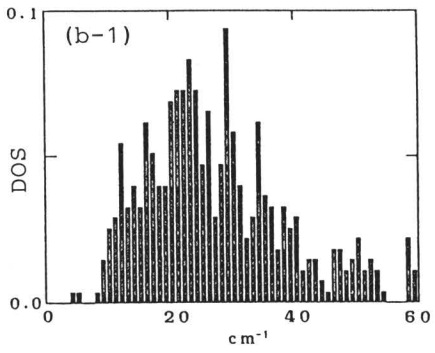
0.1
(b-1)
DOS
0.0
0
20
40
60
cm⁻¹

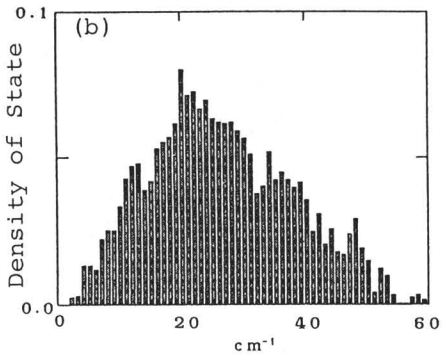
0.1
(b)
Density of State
0.0
0
20
40
60
cm⁻¹

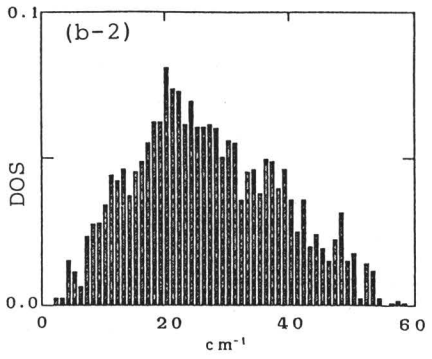
0.1
(b-2)
DOS
0.0
0
20
40
60
cm⁻¹

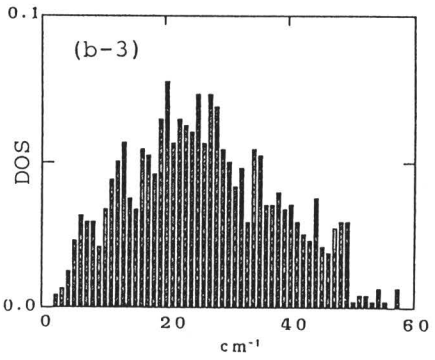
0.1
(b-3)
DOS
0.0
0
20
40
60
cm⁻¹

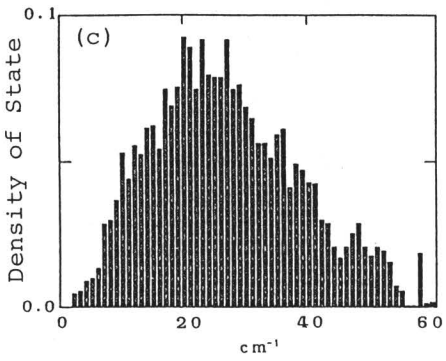
(c)
Density of State
0.1
0.0
0
20
40
60
cm⁻¹

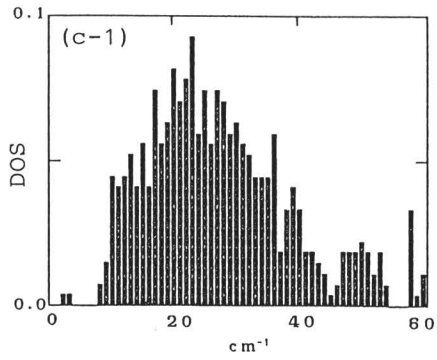
(c-1)
DOS
0.1
0.0
0
20
40
60
cm⁻¹

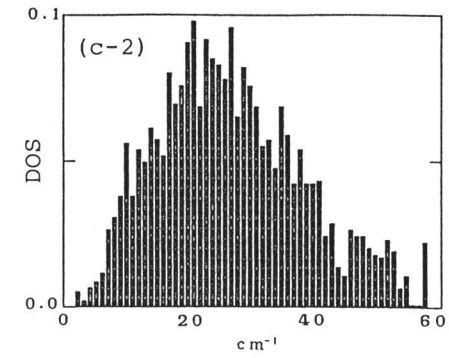
(c-2)
DOS
0.1
0.0
0
20
40
60
cm⁻¹

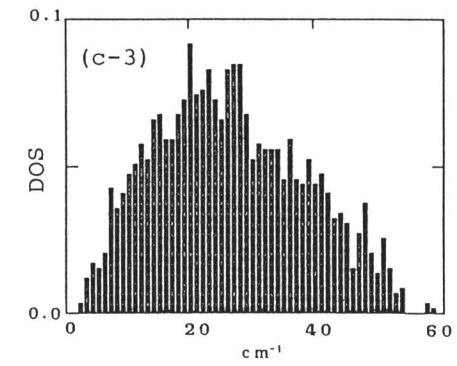
(c-3)
DOS
0.1
0.0
0
20
40
60
cm⁻¹

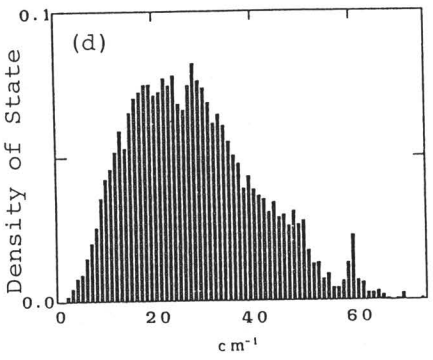
(d)
Density of State
0.1
0.0
0
20
40
60
cm⁻¹

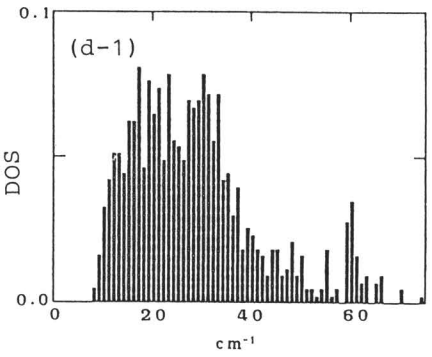
(d-1)
DOS
0.1
0.0
0
20
40
60
cm⁻¹

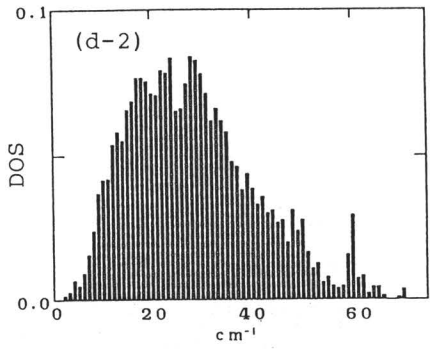
(d-2)
DOS
0.1
0.0
0
20
40
60
cm⁻¹

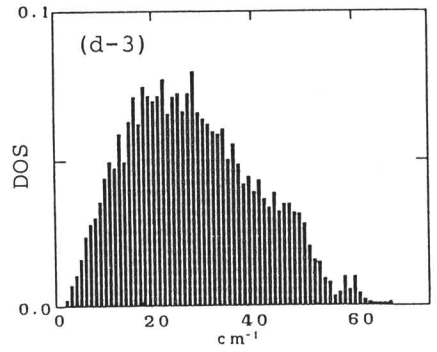
(d-3)
DOS
0.1
0.0
0
20
40
60
cm⁻¹

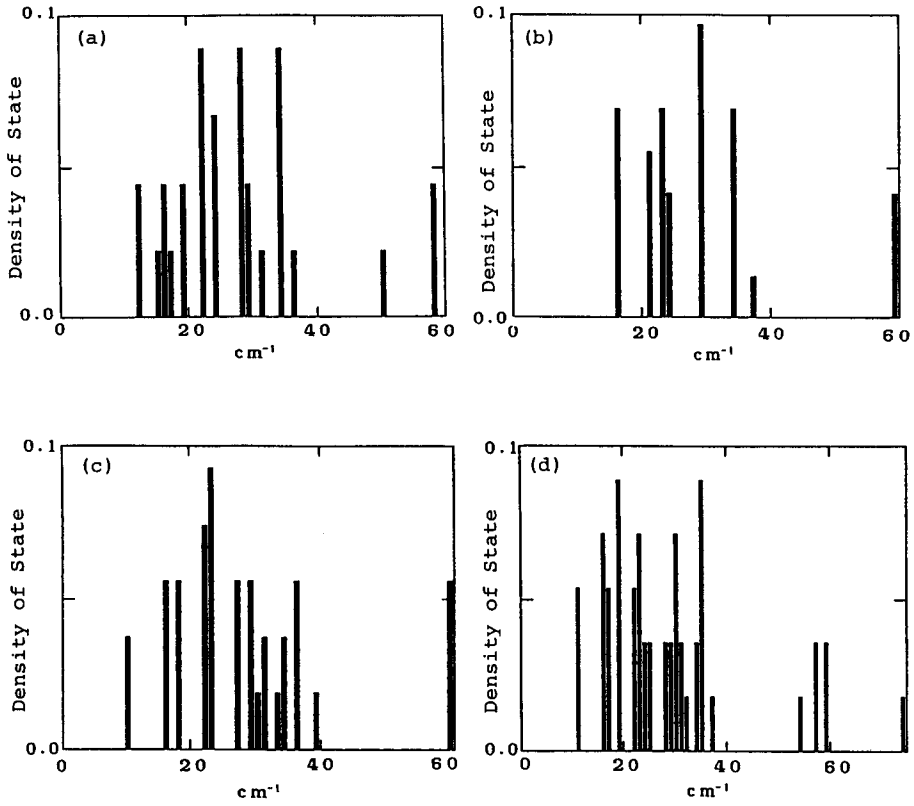

Fig. 10. Normal mode histograms for the lowest potential minimum. (a) Ar_{12}, (b) Ar_{13}, (c) Ar_{14}, (d) Ar_{19}.

such a study, we should also take the following into account: It is reported that the potential energy of the hexagonal closed-packed structure (HCP) for LJ Ar is lower than that of the corresponding FCC crystal. It is thus desirable to perform calculations for the above three structures.

5. Concluding remarks

In the present study we have carried out MD calculations of rare gas clusters composed of less than 20 molecules. We have used both LJ and LA (LJ+AT) potentials for molecular interactions. The presence of the three-body term leads to a small expansion of cluster structure at lower temperatures and a decrease in the transition temperature. These and other effects are generally of minor degree. It is thus suggested that further inclusion of a higher multi-body term might be unnecessary for rare gas clusters. The

necessity of three-body term should be emphasized when one treats free rare gas clusters at lower temperatures and when one attempts to calculate such clusters as semi-conductors and molecular clusters with strong interactions. We found some specific properties which characterize MN clusters. For clear discussions, however, we must proceed further to calculate transition states between potential minima and to consider them on the basis of the reaction rate theories. We must next study larger clusters where further complications occur as the problems of surface melting and surface diffusion. The theoretical computational studies on rare gas clusters have now been made rather extensively and emphasis will be placed in future on the above mentioned transition states and cluster kinetics based on them. Experimental studies on rare gas clusters are gradually increasing in number. It is thus hoped that further calculations should be made for the properties which can be experimentally obtained. Non-free clusters such as those in the absorbed state should also be extensively studied[19].

Acknowledgments

Most of calculations have been done at the Data Processing Center of Kyoto University. We thank Drs. Hideki Tanaka and Osamu Kitao for their discussion and encouragement.

Appendix I.

The first-order differential forms of the Axilrod-Teller potential are given here. This is necessary for the calculation of the force in MD simulation. They are necessarily neither the fastest nor the simplest ones. For other differential forms we refer to the literature[20,21].

$$\begin{aligned}\mathbf{f}_i &= -\nabla_i U_{AT}(r_{ijk}) \\ &= 3\nu(r_{ij}r_{jk}r_{ik})^{-5}\Big[\Big[(r_{jk}r_{ik})^2 - \frac{5(\mathbf{r}_{ik}\cdot\mathbf{r}_{jk})(\mathbf{r}_{ik}\cdot\mathbf{r}_{ij})(\mathbf{r}_{ij}\cdot\mathbf{r}_{jk})}{r_{ij}^2} \\ &\quad + \{(\mathbf{r}_{ij}\cdot\mathbf{r}_{jk})(\mathbf{r}_{ik}\cdot\mathbf{r}_{jk}) - (\mathbf{r}_{ik}\cdot\mathbf{r}_{ij})(\mathbf{r}_{ij}\cdot\mathbf{r}_{jk}) - (\mathbf{r}_{ik}\cdot\mathbf{r}_{jk})(\mathbf{r}_{ik}\cdot\mathbf{r}_{ij})\}\Big]\mathbf{r}_{ij} \\ &\quad + \Big[\Big[(r_{ij}r_{jk})^2 - \frac{5(\mathbf{r}_{ij}\cdot\mathbf{r}_{jk})(\mathbf{r}_{ik}\cdot\mathbf{r}_{ij})(\mathbf{r}_{ij}\cdot\mathbf{r}_{jk})}{r_{ik}^2} \\ &\quad + \{(\mathbf{r}_{ij}\cdot\mathbf{r}_{jk})(\mathbf{r}_{ik}\cdot\mathbf{r}_{jk}) + (\mathbf{r}_{ik}\cdot\mathbf{r}_{ij})(\mathbf{r}_{ij}\cdot\mathbf{r}_{jk}) + (\mathbf{r}_{ik}\cdot\mathbf{r}_{jk})(\mathbf{r}_{ik}\cdot\mathbf{r}_{ij})\}\Big]\mathbf{r}_{ik}\Big] \qquad \text{(A1)}\end{aligned}$$

$$\begin{aligned}\mathbf{f}_j &= -\nabla_j U_{AT}(r_{ijk}) \\ &= 3\nu(r_{ij}r_{jk}r_{ik})^{-5}\Big[\Big[(r_{ij}r_{ik})^2 - \frac{5(\mathbf{r}_{ik}\cdot\mathbf{r}_{jk})(\mathbf{r}_{ik}\cdot\mathbf{r}_{ij})(\mathbf{r}_{ij}\cdot\mathbf{r}_{jk})}{r_{jk}^2} \\ &\quad + \{(\mathbf{r}_{ik}\cdot\mathbf{r}_{ij})(\mathbf{r}_{ij}\cdot\mathbf{r}_{jk}) - (\mathbf{r}_{ij}\cdot\mathbf{r}_{jk})(\mathbf{r}_{ik}\cdot\mathbf{r}_{jk}) - (\mathbf{r}_{ik}\cdot\mathbf{r}_{jk})(\mathbf{r}_{ik}\cdot\mathbf{r}_{ij})\}\Big]\mathbf{r}_{jk} \\ &\quad + \Big[\Big[(r_{jk}r_{ik})^2 - \frac{5(\mathbf{r}_{ik}\cdot\mathbf{r}_{jk})(\mathbf{r}_{ik}\cdot\mathbf{r}_{ij})(\mathbf{r}_{ij}\cdot\mathbf{r}_{jk})}{r_{ij}^2} \\ &\quad + \{(\mathbf{r}_{ik}\cdot\mathbf{r}_{ij})(\mathbf{r}_{ij}\cdot\mathbf{r}_{jk}) + (\mathbf{r}_{ij}\cdot\mathbf{r}_{jk})(\mathbf{r}_{ik}\cdot\mathbf{r}_{jk}) + (\mathbf{r}_{ik}\cdot\mathbf{r}_{jk})(\mathbf{r}_{ik}\cdot\mathbf{r}_{ij})\}\Big]\mathbf{r}_{ij}\Big] \qquad \text{(A2)}\end{aligned}$$

$$\begin{aligned}\mathbf{f}_k &= -\nabla_k U_{AT}(r_{ijk}) \\ &= 3\nu(r_{ij}r_{jk}r_{ik})^{-5}\Big[\Big[(r_{ij}r_{ik})^2 - \frac{5(\mathbf{r}_{ik}\cdot\mathbf{r}_{ik})(\mathbf{r}_{ik}\cdot\mathbf{r}_{ij})(\mathbf{r}_{ij}\cdot\mathbf{r}_{jk})}{r_{ik}^2} \\ &\quad + \{(\mathbf{r}_{ik}\cdot\mathbf{r}_{jk})(\mathbf{r}_{ik}\cdot\mathbf{r}_{ij}) - (\mathbf{r}_{ij}\cdot\mathbf{r}_{jk})(\mathbf{r}_{ik}\cdot\mathbf{r}_{jk}) - (\mathbf{r}_{ik}\cdot\mathbf{r}_{ij})(\mathbf{r}_{ij}\cdot\mathbf{r}_{jk})\}\Big]\mathbf{r}_{ik} \\ &\quad + \Big[\Big[(r_{ij}r_{ik})^2 - \frac{5(\mathbf{r}_{ik}\cdot\mathbf{r}_{jk})(\mathbf{r}_{ik}\cdot\mathbf{r}_{ij})(\mathbf{r}_{ij}\cdot\mathbf{r}_{ik})}{r_{jk}^2} \\ &\quad + \{(\mathbf{r}_{ik}\cdot\mathbf{r}_{jk})(\mathbf{r}_{ik}\cdot\mathbf{r}_{ij}) + (\mathbf{r}_{ij}\cdot\mathbf{r}_{jk})(\mathbf{r}_{ik}\cdot\mathbf{r}_{jk}) - (\mathbf{r}_{ik}\cdot\mathbf{r}_{ij})(\mathbf{r}_{ij}\cdot\mathbf{r}_{jk})\}\Big]\mathbf{r}_{jk}\Big] \qquad \text{(A3)}\end{aligned}$$

Appendix II. Temperature variation of cluster structure

As is clearly seen from Fig. 3, Ar_{13} is stable and of high symmetry with a closed ICS structure. The structure of Ar_{12} could be given by the removal of just one cornered Ar atom from Ar_{13} and the structure of Ar_{14} can be obtained by putting one atom on one of the equivalent twenty triangular surfaces of Ar_{13}. Both are then naturally not so stable as Ar_{13}. Furthermore, while Ar_{19} has a stable and relatively high symmetrical structure called double icosahedron, addition or removal of one Ar atom from an Ar_{19} cluster leads to somewhat less stable structures of Ar_{18} or Ar_{20} (see Fig. 3). It is thus understood that the origin of the stability of Ar_{13} and Ar_{19} clusters can be ascribed to their highly symmetrical structure.

The structural features of clusters may be seen quantitatively by the bond length distribution function (BDF) and the angular distribution function (ADF) for the most stable structure in each cluster. The BDF is essentially the same as the radial distribution function (RDF), while the ADF is defined as the distribution of the angle at the central molecule in the triangle which is formed with two other molecules. We have obtained the results for Ar_{12}, Ar_{13}, Ar_{14} and Ar_{19} clusters. The important point is that, when the LJ model is compared with the LA model, the ADF exhibits no difference in spite of some difference in BDF. This suggests that the effect of the AT term is to expand the whole cluster without changing the fundamental structure.

Further analysis for Ar_{13} is made to compare the BDF and ADF for FCC with those for ICS structure. The results are shown in Fig. A1. Although the FCC structure is highly symmetrical, with a characteristic peak at $\sqrt{2}\ r_{min}$ in BDF, the ICS structure is generally more stable than the FCC structure. The former has a smaller surface energy and the distance between the central and surface molecules. On the other hand, the ICS structure has the characteristic peaks of ADF at 60° and 120°, while an extra peak, characteristic to the FCC structure, is also seen at 90°. This peak can be used as an evidence for the noncrystal to crystal transition in cluster structures. The energy difference between ICS and FCC structures becomes smaller when the three-body term is added. This suggests that the three-body term is important when we examine the size of cluster at which the conversion from ICS to FCC will occur. The contribution of the

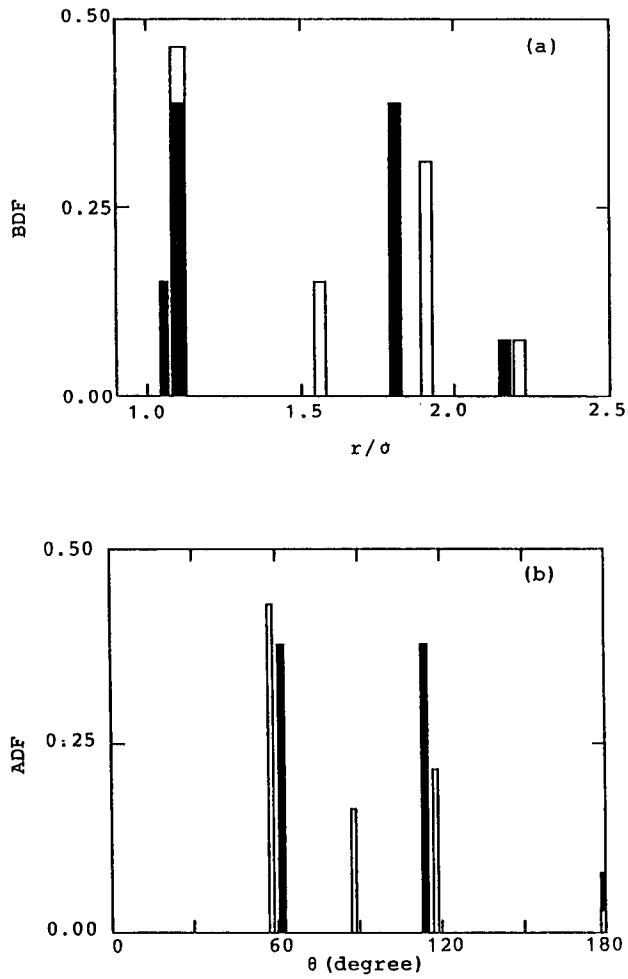

Fig. A1. Comparison between the ICS and FCC structures of Ar_{13}. Black: ICS. White: FCC.
(a) Bond length distribution function
(b) Angular distribution function

three-body term to the total potential energy of the cluster at 0 K is 3.5 to 5.0%. This is to be compared with the value 4.5 to 5.5% for that in the case of the bulk phase.

The variations of the BDF and ADF for some Ar clusters (Ar_{12}, Ar_{13}, Ar_{14} and Ar_{19}) with temperature have been examined. The temperatures used are 3, 13 and 34 K, respectively. It is clearly seen from the temperature variation that the BDF changes from a solid-like structure at a lower temperature to a liquid-like structure at a higher temperature. The general tendency is the same for both the LJ and LA models. However, there are small differences in the position and height of the BDF peaks. While

the change in the peak height is not so important, the shifts of the second peak to a longer distance are worth mentioning. This reflects the difference in the fundamental structure

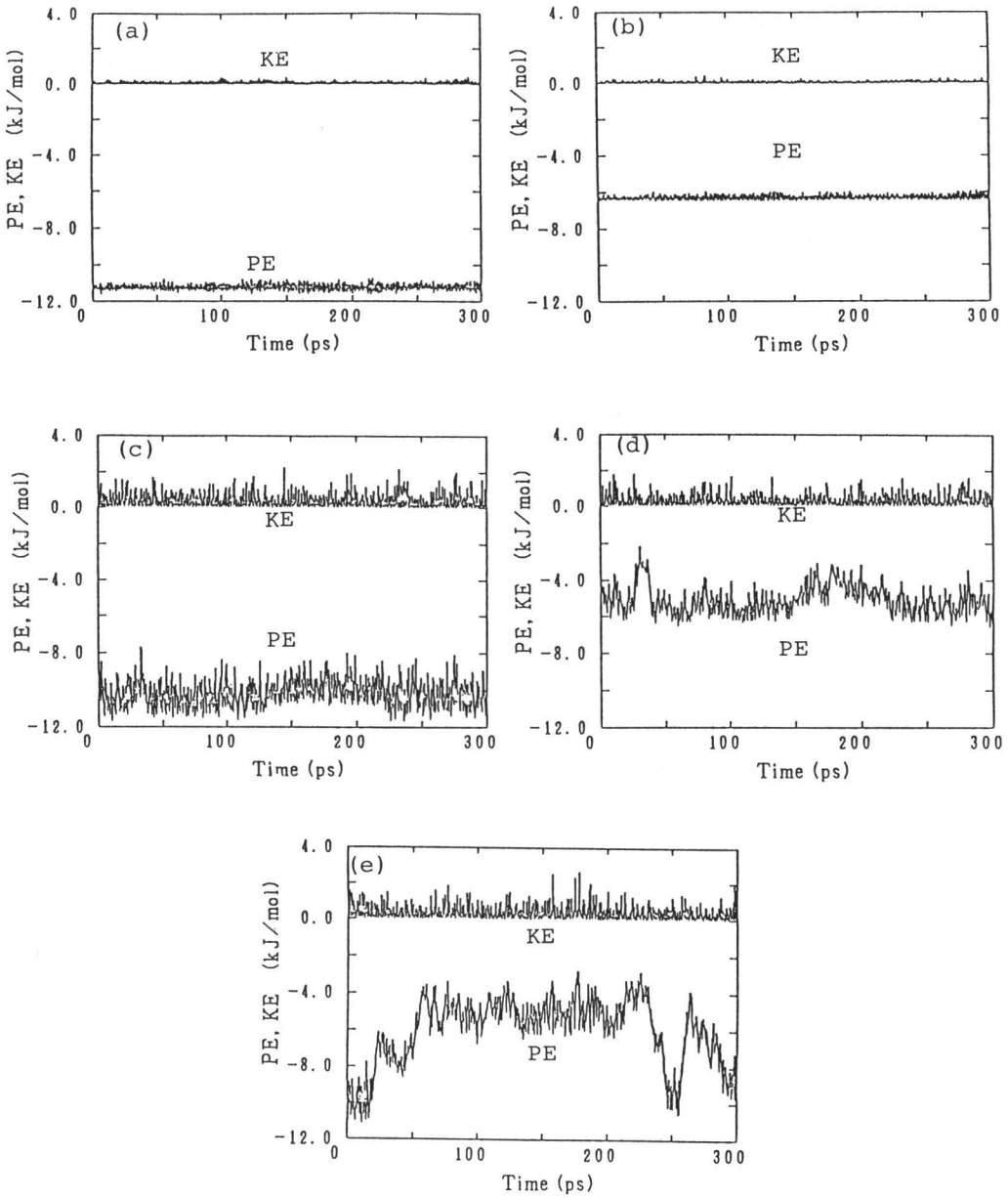

Fig. A2. The kinetic and potential energies of one particle in Ar_{13} cluster with the LJ potential.
(a), (b) T=5 K (c), (d) T=33 K (e) T=35 K

at lower temperature. At higher temperatures the influence of the AT potential on structure is almost negligible, probably because this potential is rather weak and of short range nature.

On the other hand, the ADF changes appreciably with temperature. The peaks at 60° and 120° are significant for the ADF at lower temperatures and, as the temperature increases, a minor peak near 90° appears. Again, there is essentially no difference between the LJ and LA models, though minor difference is seen at higher temperatures. A stronger three-body term enhances this tendency. One of the reasons might be the frequent reorganizations of molecular configuration as in the liquid phase. Such effects

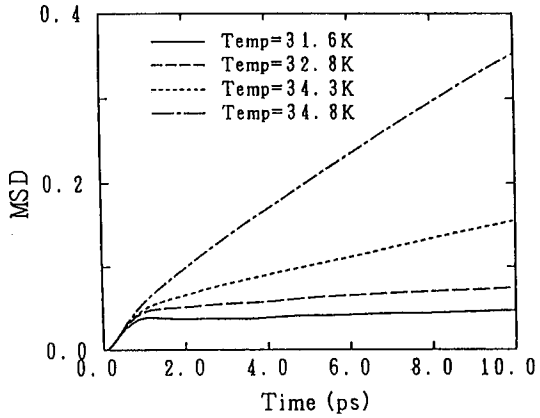

Fig. A3. Mean square displacement (MSD) of Ar_{13} cluster with LJ potential at several temperatures.

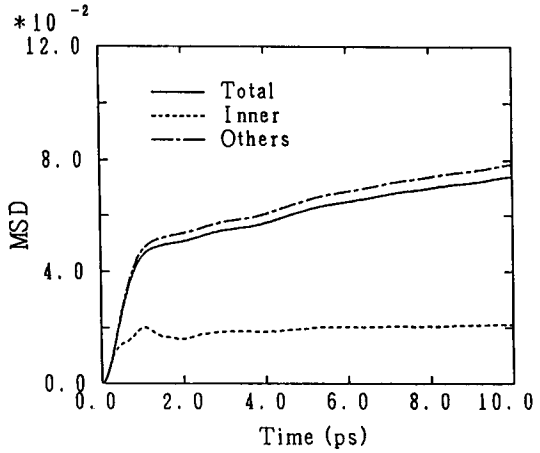

Fig. A4. Mean square displacement (MSD) calculated separately for inner particles and other particles in Ar_{13} cluster at T=32.8 K.

may be dependent on the three-body potential. However, the BDF has no relation with such configurational changes, as the cluster diameter remains unchanged. In Fig. A2 it is shown how the structural changes in Ar_{13} clusters occur with the increase in temperature. At a lower temperature of 5 K, both the potential and kinetic energies fluctuate only slightly, suggesting the presence of only a minor vibration-like motion. The fluctuation becomes larger as the temperature rises to 20 K, but no appreciable structural change is observed (not shown in Fig. A2). The energetic fluctuation becomes fairly large at 33 K and some of the surface molecules have higher potential energies. This is evidence for the movement of surface molecules. At 35 K, even the exchange of central molecules is observed, indicating a large structural change. This is closely related to the phase transition explained later.

Such molecular motion may be seen from the temperature variation of the mean

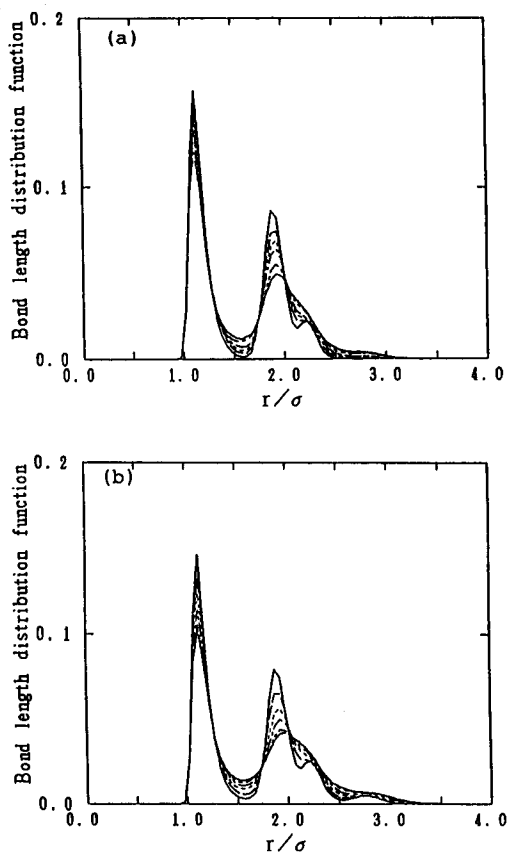

Fig. A5. Bond length distribution function at several temperatures in the transition region.
(a) Ar_{13} (b) Ar_{14}

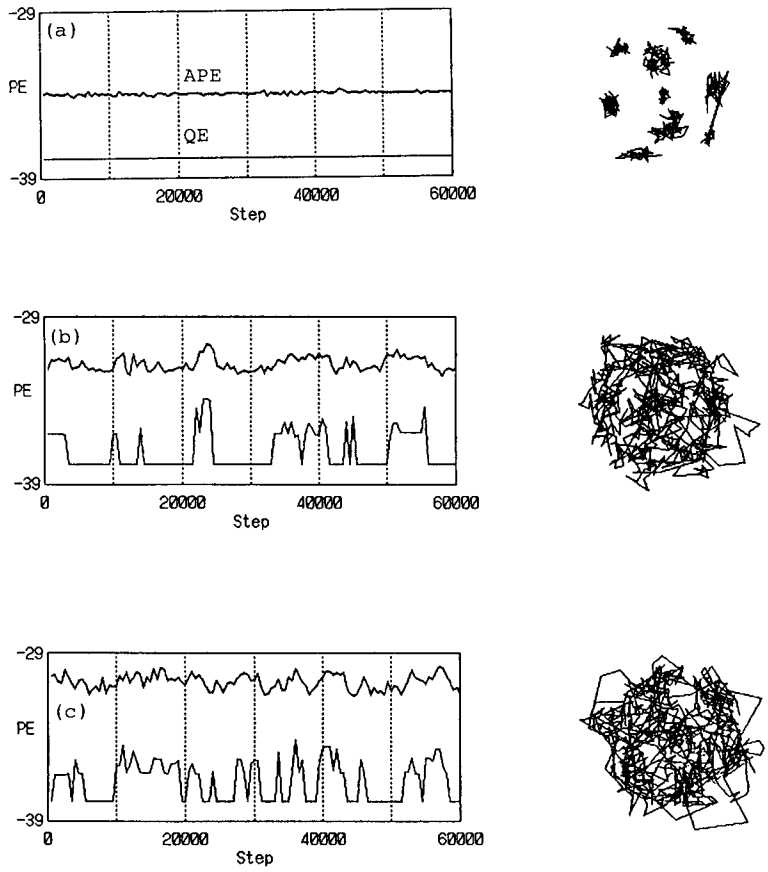

Fig. A6. Averaged potential energy (APE) and quenched energy (QE) *vs* time and the trajectories of clusters.
(a) Ar_{12}, T=24.5 K (b) Ar_{12}, T=29.2 K (c) Ar_{12}, T=31.2 K (d) Ar_{13}, T=29.2 K (e) Ar_{13}, T=32.8 K (f) Ar_{13}, T=33.6 K (g) Ar_{14}, T=28.5 K (h) Ar_{14}, T=33.9 K (i) Ar_{14}, T=36.3 K (j) Ar_{19}, T=29.7 K (k) Ar_{19}, T=31.4 K (l) Ar_{19}, T=33.5 K

square displacement (MSD) of each particle in the cluster. Only the case of the LJ model is shown in Fig. A3. While this is an average over all the particles, Fig. A4 shows MSD's separately for the central particle and those near the surface. It is clear that, though the central particle does not move, the surface molecules begin to move. This might be closely related to the phenomena of surface diffusion and melting in larger clusters. The same is true for neighboring non-MN clusters such as Ar_{12} and Ar_{14}. Since they are not of closed from, surface particles tend to move frequently even at fairly lower temperatures.

Finally, we estimate that the contribution of the three-body term to the potential energy is 4.0–4.5% at lower temperatures and 3.0–4.0% at higher temperatures.

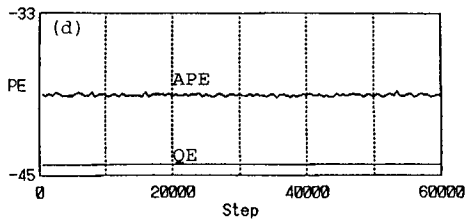

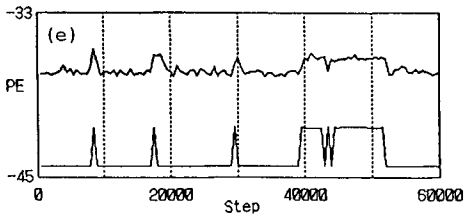

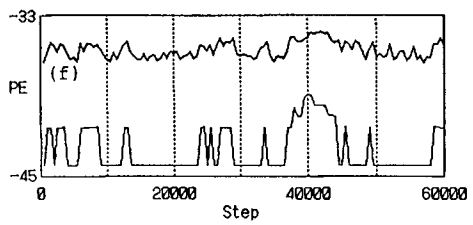

Appendix III. Detailed analysis of transition region

In this Appendix, detailed analyses are made for the transitions in the Ar_{13} MN cluster, and Non-MN Ar_{12} and Ar_{14} clusters with the LJ potential. In view of the minor effect of the three-body term, no calculation is made for the clusters with the LA potential. We adopt the method proposed by Berry et al[11]. The temperature ranges studied are respectively, 30 to 35 K for Ar_{13}, 24 to 37 K for Ar_{12} and 28 to 38 K for Ar_{14} clusters.

The temperature dependence of BDF is shown for Ar_{13} and Ar_{14} clusters in Fig. A5. It is seen that, as the temperature increases, the splitting of the second peak disappears and the distributions in the first minimum and tail appear. This means that the cluster structure changes rather continuously. To examine this in more detail, the change in the

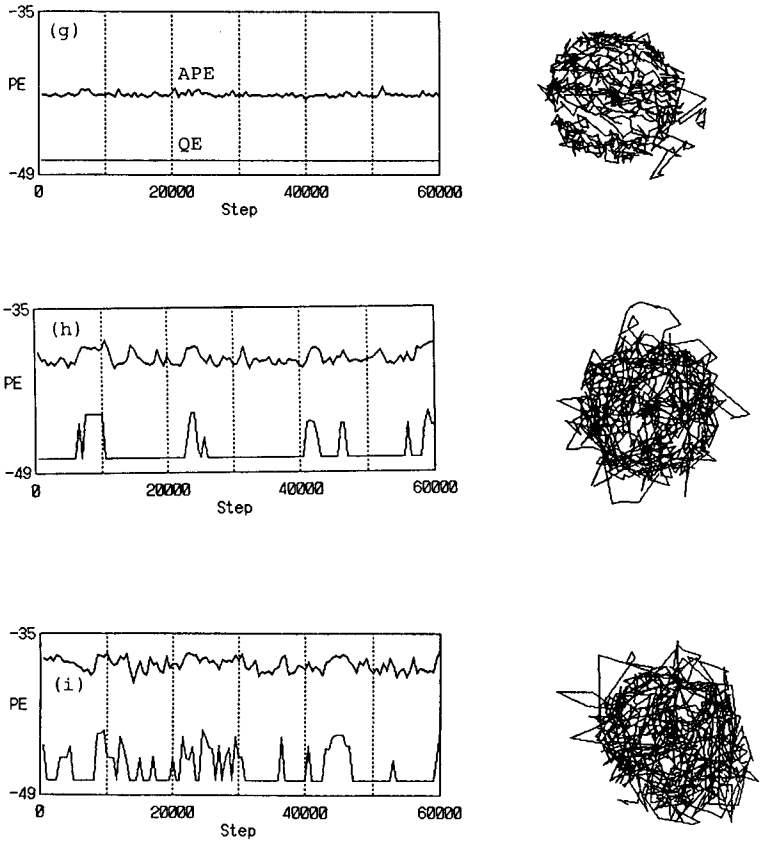

potential energy of the systems is monitored. As shown in Fig. A6, the potential energy changes largely and frequently. To remove minor vibrational change, we examine the change in the average potential energy (APE) which is defined as an average over 500 time steps. Trajectories of each particle are also shown in Fig. A6.

It is seen in Fig. A6 that the APE for Ar_{13} does not show appreciable change at lower temperature but seems to have two levels at about 33 K. At higher temperatures, two levels cannot be distinguished. The particle motion is such that only lattice vibration occurs at lower temperatures and that the vibration is overlapped by translation (diffusion) at higher temperatures.

We examine the case of 33 K in more detail. When the APE is nearly constant, molecules vibrate around each lattice site. However, when the APE shows appreciable change, trajectories of some particles extend from the original lattice site, leading to a structural change. On the other hand, the presence of two levels is observed for Ar_{12} and

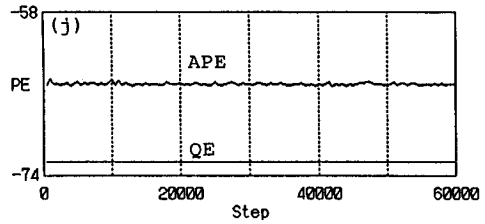

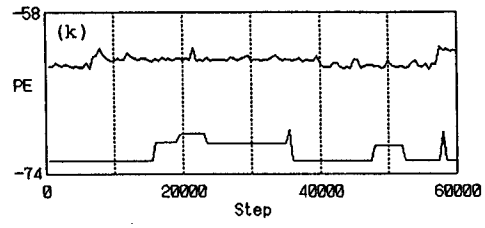

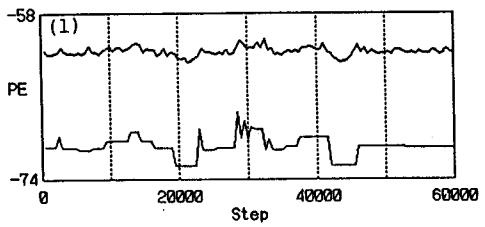

Ar_{14}, though the difference between the levels is not so large as that for Ar_{13}. However, even though only one level in the APE can be seen at lower temperatures, trajectories of particles are not like lattice vibrations. This is due to the fact that Ar_{12} and Ar_{14} are not of closed form; in other words, the particle motion below 30 K is affected by a defect on the surface or one particle attached to the smooth surface. The distribution function for APE has been calculated as in Fig. A7. In accordance with the two energy levels mentioned above, the distribution aplits into two large peaks. Thus, the BDF can be calculated separately for the two regions in the distribution as in Fig. A8. For this purpose, we calculate the average potential energy for 100 time steps, examine to which level this region belongs, and then calculate the BDF by using averaged coordinates for these 100 time steps. In the cases of Ar_{12} and Ar_{14}, these two BDF's do not show any appreciabble difference. For Ar_{13}, however, the situation is somewhat different. There are differences in the first minimum and the long tail. While the distribution is solid-like for the higher energy region, that for the lower energy region is liquid-like. This indicates

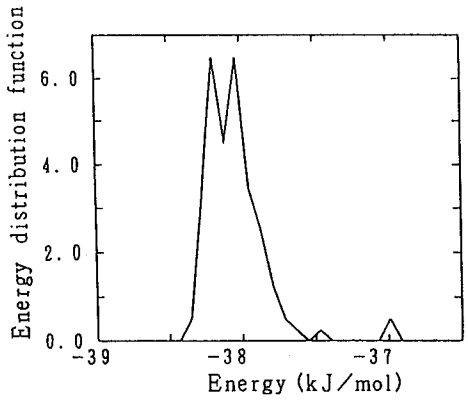

Fig. A7. The distribution function of the averaged potential energy for Ar_{13}.

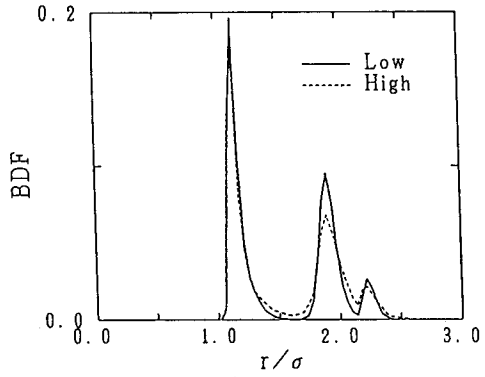

Fig. A8. Bond length distribution functions calculated for low and high energy regions.

that there is a coexistence of these two states, solid-like and liquid-like, in one run of MD simulation[11d]. Such an observation of two different levels in the APE distribution largely reflects the details of potential energy surface[11e]. We thus attempt to apply the quenching technique to our cluster systems.

References

[1] O. Echt, K. Sattler and E. Recknagel, Phys. Rev. Lett., **476**, 1121 (1981).
[2] I. A. Harris, R. S. Kidwell and J. A. Northby, Phys. Rev. Lett., **53**, 2390 (1984).
[3] (a) J. Farges, B. Raoult and G. Torchet, J. Chem. Phys., **78**, 5067 (1983); (b) J. Farges, M. F. de Feraudy, B. Raoult and G. Torchet, *ibid.* **84**, 3491 (1986).
[4] D. J. McGinty, J. Chem. Phys., **58**, 4733 (1973).
[5] C. L. Briant and J. J. Burton, J. Chem. Phys., **63**, 2045 (1975).
[6] (a) R. D. Etters and J. B. Kaelberer, Phys. Rev. A, **11**, 1068 (1975); (b) J. B. Kaelberer and R. D. Etters, J. Chem. Phys., **66**, 3233 (1977); (c) R. D. Etters and J. B. Kaelberer, *ibid.* **66**, 5112 (1977).

[7] N. Quirk and P. Sheng, Chem. Phys. Lett., **110**, 63 (1984).
[8] (a) M. R. Hoare and P. Pal, Adv. Phys., **20**, 161 (1971); **24**, 645 (1975); (b) M. R. Hoare and J. A. Mcinnes, *ibid.* **32**, 791 (1983).
[9] J. W. Lee and G. D. Stein, J. Phys. Chem., **91**, 2450 (1987).
[10] J. Xie, J. A. Northby, D. L. Freeman and J. D. Doll, J. Chem. Phys., **91**, 612 (1989).
[11] (a) J. Jellinek, T. L. Beck and R. S. Berry, J. Chem. Phys., **84**, 2783 (1986); (b) F. G. Amar and R. S. Berry, *ibid.* **85**, 5943 (1986); (c) H. L. Davis, J. Jellinek and R. S. Berry, *ibid.* **86**, 6456 (1987); (d) T. L. Beck, J. Jellinek and R. S. Berry, *ibid.* **87**, 545 (1987); (e) T. L. Beck and R. S. Berry, *ibid.* **88**, 3910 (1988).
[12] D. J. Wales, J. Am. Chem. Soc., **112**, 7908 (1990).
[13] J. Uppenbrink and D. J. Wales, J. Chem. Phys., **96**, 8520 (1992).
[14] B. M. Axilrod and E. Teller, J. Chem. Phys., **11**, 299 (1943).
[15] L. Verlet, Phys. Rev., **159**, 98 (1967).
[16] F. H. Stillinger and T. A. Weber, Phys. Rev. A, **25**, 978 (1982).
[17] J. D. Honeycutt and H. C. Andersen, J. Phys. Chem., **91**, 4950 (1987).
[18] (a) R. S. Berry, H. L. Davis and T. L. Beck, Chem. Phys. Lett., **147**, 13 (1988); (b) D. J. Wales, J. Chem. Phys., **91**, 7002 (1989).
[19] V. V. Nauchitel and A. J. Pertsin, Mol. Phys., **40**, 1341 (1980).
[20] C. Hoheisel, Phys. Rev. A, **23**, 1998 (1981).
[21] M. P. Allen and D. J. Tildesley, *Computer Simulation of Liquids* (Oxford Univ. Press, New York, 1987).